Synergistic effect of photoanode and photocathode modified with oxygenated multi-walled carbon nanotubes in dye-sensitized solar cells

Min-Jung Song* and Joon-Hyung Jin**,†

*Department of Nano Convergence Engineering, Seokyeong University, 124 Seokyeong-ro, Sungbuk-gu, Seoul 02713, Korea
**Department of Chemical Engineering, Kyonggi University, 154-42 Gwanggyosan-ro,
Yeongtong-gu, Suwon, Gyeonggi 16227, Korea

Abstract−Oxygenated multi-walled carbon nanotubes (OMWNTs) were employed as additives in conventional TiO_2-based photoanodes and platinum-free conducting polymer-based photocathodes. The OMWNTs were induced to form covalent bonds with TiO_2 nanoparticles (NPs) and were successfully intercalated into a poly (3, 4-ethylenedioxythiophene)-polystyrene sulfonate (PEDOT:PSS) network. Furthermore, a dye-sensitized TiO_2-OMWNT-based photoanode and a PEDOT:PSS-OMWNT-based electrocatalytic photocathode were both assembled into a photoelectrochemical cell. Replacing the typical platinized photocathode with PEDOT:PSS-OMWNTs enhances the energy conversion efficiency by approximately 13.9% when compared to a typical dye-sensitized solar cell composed of $FTO/TiO_2/N719//Pt/FTO$. Similarly, a 25.6% increase in efficiency was observed by a spray-coated TiO_2-OMWNT layer as the photoanode instead of simple anatase TiO_2 NPs. In addition, 42.9% higher efficiency was achieved by utilizing the two OMWNT-modified electrodes together. This excellent performance is attributed to the synergistic effect of the OMWNT-modified photoanode and photocathode. This may be related to the effective suppression of unwanted back transport and recombination reactions.

Keywords: Dye-sensitized Solar Cell, Oxygenated Multi-walled Carbon Nanotubes, PEDOT:PSS, Platinum-free Counter Electrode, TiO_2

INTRODUCTION

Dye-sensitized solar cells (DSSCs) have proven to be excellent candidates for next-generation solar cells owing to their low cost, relatively low CO_2 emission, and high energy conversion efficiency (η) [1]. DSSCs have three parts: a photoanode (working electrode), an electrolyte, and a photocathode (counter electrode). TiO_2 is the most widely utilized photoanode material because of its high photoelectric conversion efficiency, photochemical stability, non-toxicity, and abundance for mass production. Many experimental studies have been conducted to enhance the efficiency of DSSCs by modifying specific TiO_2 nanostructures [2-4] by surface post-treatment, coating treatment, or incorporation with carbon [5-7], noble metal nanomaterials [8-10], and element doping [11-14]. The counter electrode also plays a significant role in the reduction of I_3^- ions generated from the oxidation of I^- ions on the photoanode. Because transparent conducting glass substrates (e.g., fluorine-doped tin oxide; FTO) have less catalytic activity toward I_3^- reduction and a high overpotential for charge transfer, a catalytic layer on FTO substrates such as platinum is required. Even though Pt exhibits excellent catalytic activity, excellent conductivity, and chemical stability, high material or fabrication cost for the Pt layer limits its widespread use [15,16]. Many researchers have attempted to develop low-cost alternatives for high-performance DSSCs, such as carbonaceous materials, including graphene or carbon nanotubes (CNTs) and organic polymeric conductors.

Poly(ethylene-3,4-dioxythiophene):poly(styrene sulfonate) (PEDOT: PSS), which is a conductive co-polymer, has been widely used in thin-film organic optoelectronic and photovoltaic devices because of its high electrical conductivity, cost-effectiveness, and good film-forming ability [17]. However, pristine PEDOT:PSS films have a lower catalytic performance than Pt thin films.

CNTs are frequently used additives for preparing hybrid materials owing to their low resistivity, high chemical stability, and mechanical strength. CNT-based hybrid materials can provide a high surface-to-volume ratio, enhanced conductivity, and electrocatalytic activity [18]. Owing to their unique properties, CNTs have been widely used as additives in DSSCs to enhance the performance of TiO_2-based photoanodes and electrocatalytic photocathodes [19]. Some research groups have reported DSSCs based on CNTs with various TiO_2 nanocomposites: for example, nanoparticles [20], nanowire array films [19], and nanotube arrays [21]. In particular, DSSCs incorporating oxygenated multi-walled CNTs (OMWNTs) into the working or counter electrodes exhibit significantly improved performance because carboxylic acid groups on the OMWNT surface created by O_2 plasma treatment lead to a stronger Ti-O-C bond between the OMWNTs and the TiO_2 nanoparticles at the working electrode than in conventional MWNTs. In addition, OMWNTs show better compatibility with the positively charged PEDOT-based photocathode than bare MWNTs. Our previous work showed that

photoelectrochemical cells equipped with OMWNT-decorated photoanodes provided photogenerated electrons with a more reliable and faster route to the photoanode, faster electron transport due to enhanced conductivity of the polymer network, and improved electrocatalytic activity for the I^-/I_3^- redox reaction on the photocathode [22,23].

In this work, we prepared a polymer composite of OMWNT-intercalated PEDOT:PSS network (PEDOT:PSS-OMWNTs) as the photoanode of a DSSC and a functional hybrid material of OMWNT-decorated TiO_2 nanopowder (NPs) (TiO_2-OMWNTs) as the photocathode, and applied both OMWNT-based electrodes in DSSCs at the same time. By combining the OMWNT-intercalated TiO_2 NPs as the photoanode and the OMWNT-decorated PEDOT:PSS network as the photocathode, the newly devised DSSC exhibited a synergistically improved performance.

EXPERIMENTAL

1. Reagents and Materials

The MWNTs (CM-100; diameter=10-15 nm) and TiO_2 NPs (Degussa P25, diameter=20 nm) were obtained from Hanwha Nanotech Co. (Seoul, Korea) and Nanoshel LLC (Wilmington, USA), respectively. 1,2-dichlorobenzene, poly(styrene sulfonate) (PSS), poly(3,4-ethylenedioxythiophene) (PEDOT), 1,2-dimethyl-3-N-propylimidazolium iodide, iodine, lithium iodide, and 4-tert-butylpyridine were purchased from Sigma-Aldrich Chemicals (St. Louis, MO, USA). FTO (resistivity=7 Ω/sq, transmittance >81%) was prepared by Woo Yang Co. (Busan, Korea). Pt paste (Platisol T/SP) and N719 (Ruthenizer 535-bisTBA) dyes were obtained from Solaronix SA Co. (Aubonne, Switzerland). Surlyn 1715 (thickness=60 μm) as an ionomer film was purchased from DuPont Co., Ltd. (Delaware, USA).

2. Preparation of the OMWNT-intercalated Photoanode

For the photoanode, evenly distributed oxygen-containing chemical functional groups, such as carboxylic acid groups on the surface of OMWNTs, enable strong bond formation with a high bond dissociation energy between the OMWNTs and TiO_2 NPs. The solution for spray-coating the photoanode contained 0.02 wt% OMWNTs, TiO_2 NPs, and 1,2-dichlorobenzene as a solvent. After spray-coating the OMWNT-intercalated TiO_2 layer on the FTO substrate, the resulting anodic thin film was annealed and sensitized with N719 dye to obtain FTO/TiO_2-OMWNTs/N719.

3. Preparation of the OMWNT-decorated Photocathode

The OMWNTs were intercalated into PEDOT:PSS film during anodic electropolymerization of the PEDOT:PSS on an FTO substrate in an aqueous medium containing 0.1 M PSS (30% in H_2O), 0.01 M PEDOT (97%), and the OMWNTs. The PEDOT:PSS-OMWNT hybrid layer was deposited on the FTO surface by cyclic voltammetry in the range of -0.8-1.2 V at a scan rate of 100 mV s^{-1}. The small capacitive current observed during electropolymerization confirms that a thin conducting polymer film is formed on the FTO surface. More detailed information concerning the photoanode and photocathode preparation is available elsewhere [7,22]. A platinized FTO electrode was also prepared for comparison by spin coating (6,000 rpm for 1 min) and annealing (450 °C for 10 min) of Pt paste.

4. Assembly of Dye-sensitized Solar Cells with Various Electrode Components

Two different photoanodes (FTO/TiO_2-OMWNTs/N719 and FTO/TiO_2/N719) and photocathodes (FTO/Pt and FTO/PEDOT:PSS-OMWNTs) were prepared, and four photoelectrochemical cell systems were obtained: DSSC1 (for FTO/TiO_2/N719//Pt/FTO), DSSC2 (for FTO/TiO_2/N719//PEDOT:PSS-OMWNTs/FTO), DSSC3 (for FTO/TiO_2-OMWNTs/N719//Pt/FTO), and DSSC4 (for FTO/TiO_2-OMWNTs/N719//PEDOT:PSS-OMWNTs/FTO). The OMWNTs for both the photoanode and photocathode were prepared previously by functionalizing the MWNTs with laboratory-made O_2 plasma equipment. The plasma process was optimized to meet the requirements of the photoanode or photocathode by controlling the plasma power and plasma treatment time [23]. The electrode components were combined using the ionomer film. The organic electrolyte phase contained 0.6 M 1,2-dimethyl-3-N-propylimidazolium iodide, 0.05 M I_2, 0.1 M LiI, and 0.5 M 4-tert-butyl-pyridine in acetonitrile.

RESULTS AND DISCUSSION

Fig. 1 shows a schematic illustration of the working mechanism of DSSC4. When the photoanode is exposed to light, photoelectrons are generated from the sensitizer molecules. These electrons are injected into the conduction band of TiO_2 nanoparticles and are eventually collected by the photoanode, and at the same time, holes move towards the photocathode through the electrolyte phase containing the I^-/I_3^- redox couple. Eventually, the harvested electrons move further through an external circuit and reach the photocathode, where triiodide is electrocatalytically reduced to iodide [24]. Because the OMWNT content in the DSSC can affect the film transparency of the conducting oxide electrode, recombination of the harvested electrons, and back transport of the electrons to triiodides, the amount of OMWNTs in the active materials for both the photoanode and cathode was carefully optimized, as shown in Fig. S1. The photocurrent density versus voltage (J-V) curves of the various photoanodes (Fig. S1(a)) and photocathodes (Fig. S1(b)) indicate that the photoanode containing 0.02 wt% OMWNTs and
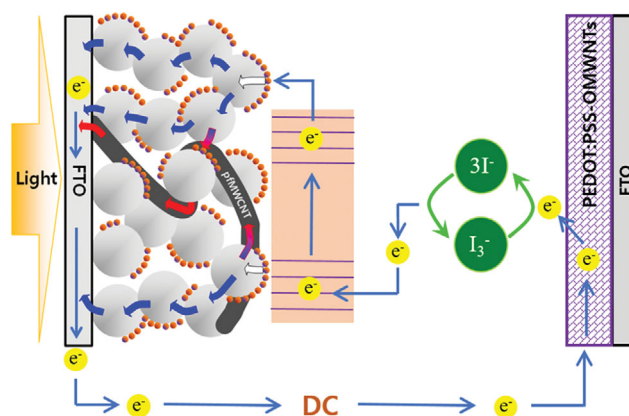

Fig. 1. Schematic illustration of the DSSC principle on a PEC consisting of FTO/TiO_2-OMWNTs/N719//FTO/PEDOT:PSS-OMWNTs.
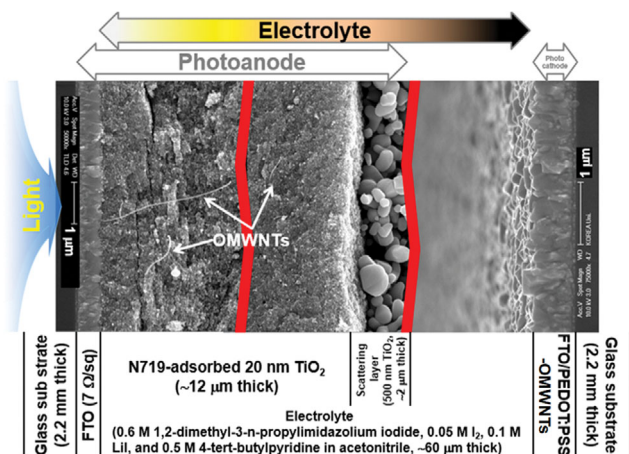
Fig. 2. SEM images of a modified PEC that consists of FTO/TiO$_2$-OMWNTs/N719//FTO/PEDOT:PSS-OMWNTs.

Fig. 4. J-V characteristic curve of (a) DSSC1, (b) DSSC2, (c) DSSC3, and (d) DSSC4 under illumination with an air mass of 1.5 (100 mW cm^{-2}) using a 150 W xenon lamp. Note that the lamp power was calibrated with a Si reference solar cell.

the photocathode containing 0.002 wt% OMWNTs showed the best results in terms of η.

Fig. 2 shows SEM images of the DSSC4 system. The photoanode is composed of a 2-μm TiO$_2$ scattering layer, a 12-μm OMWNT-TiO$_2$ composite layer, and a 580-nm FTO layer on a 2.2-mm glass substrate. A PEDOT:PSS-OMWNT hybrid film in the photocathode was successfully formed on the FTO surface with a thickness of approximately 750 nm. These conducting polymer films and MWNTs enhance the electrochemically active area and act as a catalytic layer for the reduction of triiodide [22]. A stronger Ti-O-C bond is formed between the OMWNTs and the TiO$_2$ nanoparticles, owing to the presence of many carboxylic acid groups on the MWNT surface, which provides a more reliable and faster route for the photogenerated electrons to the photoanode [7].

CV diagrams of the PEDOT:PSS-OMWNT hybrid film on FTO and platinized FTO electrodes were obtained at a scan rate of 100 mV s^{-1} in an acetonitrile solution containing 10 mM LiI, 1 mM I$_2$,
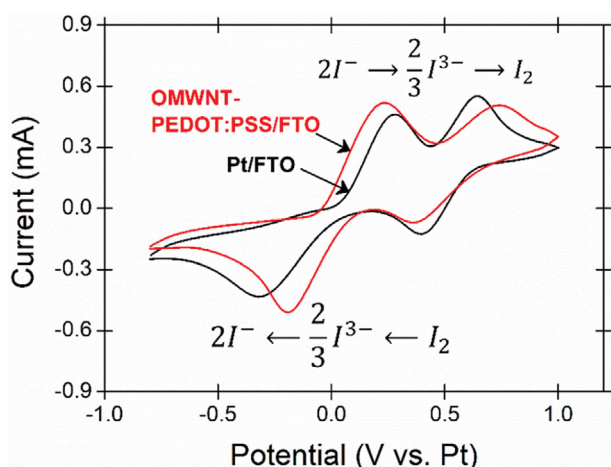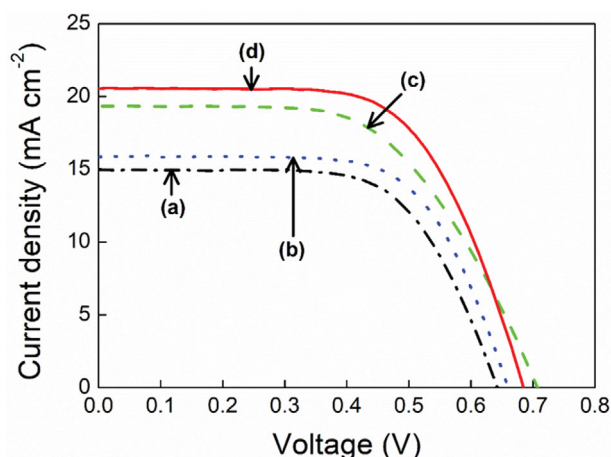

Fig. 3. Cyclic voltammogram of PEDOT:PSS-OMWNTs hybrid film on FTO in a CH$_3$CN solution containing 10 mM LiI, 1 mM I$_2$, and 0.1 M LiClO$_4$ at a scan rate of 100 mV s^{-1}. Note that the cyclic voltammogram of the platinized FTO electrode is also shown for comparison.

and 0.1 M LiClO$_4$ to compare the chemical stability of the PEDOT:PSS-OMWNT-based counter electrode in a corrosive I^-/I_3^- redox system to that of a typical Pt electrode. As shown in Fig. 3, two oxidation events for the I^-/I_3^- redox couple on the OMWNT-PEDOT:PSS/FTO electrode are observed: iodide is oxidized to triiodide at 0.233 V and further oxidized to form iodine at 0.742 V versus the Pt quasi-reference electrode. In the reverse potential scan, iodine is reduced back to triiodide at 0.364 V, eventually forming iodide at 0.195 V. The difference between the peak potential for the oxidation and reduction processes of the PEDOT:PSS-OMWNT electrode is 0.509 and 0.559 V, respectively. Compared to those of the platinized FTO electrode showing 0.364 V for oxidation and 0.718 V for reduction, the PEDOT:PSS-OMWNT electrode provides better stability with less than 10% difference in peak potential separation for redox processes. Notably, the PEDOT:PSS-OMWNT electrode allows a much faster reduction process with a narrower peak potential separation than the platinized electrode.

Fig. 4 presents the J-V characteristics of various DSSCs under illumination with an air mass of 1.5 (AM 1.5), and 100 mW cm^{-2}. The photovoltaic parameters of each DSSC are summarized in Table 1. The J-V curve of DSSC3 indicates that the OMWNT-intercalated TiO$_2$ layer increases the transfer rate of the photoelectrons more effectively, showing a η value 25.4% higher than that for DSSC1, which comprises a conventional FTO/TiO$_2$/N719 based working electrode and an FTO/Pt counter electrode. Anchored OMWNTs in the TiO$_2$ NP layer are helpful for the effective transport of photoelectrons by improving the polarizability and conductivity of the light-sensitive layer. As a result, an increased open-circuit potential (V$_{oc}$) and short-circuit current density (J$_{sc}$) are observed at the expense of the fill factor (FF).

The OMWNTs also enhanced the electrocatalytic activity of the conducting polymer-based counter electrode. An increase of approximately 11.1% in η value can be achieved by adding OMWNTs to the PEDOT:PSS-based counter electrode, which was verified by comparing the J-V curve of DSSC2 with that of DSSC1. The OMWNTs provide the PEDOT:PSS-based photocathode with comparable or

Table 1. Photovoltaic parameters of the various DSSCs

Structure		V_{oc} [V]	J_{sc} [mA cm^{-2}]	FF	η [%]
DSSC1	FTO/TiO$_2$/N719//Pt/FTO	0.64	15	65	6.3
DSSC2	FTO/TiO$_2$/N719//PEDOT:PSS-OMWNTs/FTO	0.68	16	66	7.0
DSSC3	FTO/TiO$_2$-OMWNTs/N719//Pt/FTO	0.71	19	57	7.9
DSSC4	FTO/TiO$_2$-OMWNTs/N719//PEDOT:PSS-OMWNTs/FTO	0.68	21	64	9.0

even improved electrocatalytic activity, which is essential for the I_3^-/I^- redox reaction.

The combination of both OMWNT-decorated photoanode and cathode together, i.e., DSSC4, increases the η value by approximately 42.9% (comparing the J-V curve of DSSC4 with that of DSSC1), which is 6.4% more than one can expect simply from the sum of 11.1% and 25.4%. These results lead us to consider a synergistic effect of the use of OMWNTs for both the photoanode and photocathode. The fact that the DSSC comprising both FTO/TiO$_2$-OMWNTs/N719 and FTO/PEDOT:PSS-OMWNTs displays the best PEC performance is mainly attributed to the increased J_{sc} value. In addition, the simultaneous use of the OMWNT-based photoanode and cathode recovers the fill factor to an extent comparable to that of the traditional DSSC1.

The synergistic effect of the combination of the two OMWNT-decorated electrodes seems to be due to the effective suppression of back transport and recombination reactions, which was previously confirmed by the large increase in J_{sc} for DSSC4 (about a 40% increase compared to that of DSSC1). An electrochemical impedance spectroscopy (EIS) study of the various DSSCs was performed under dark conditions with a DC bias potential of -0.79 V, a step potential of 5 mV, and a frequency range from 100 mHz to 100 kHz. The EIS spectra, shown in Fig. 5, reveal reduced semicir-
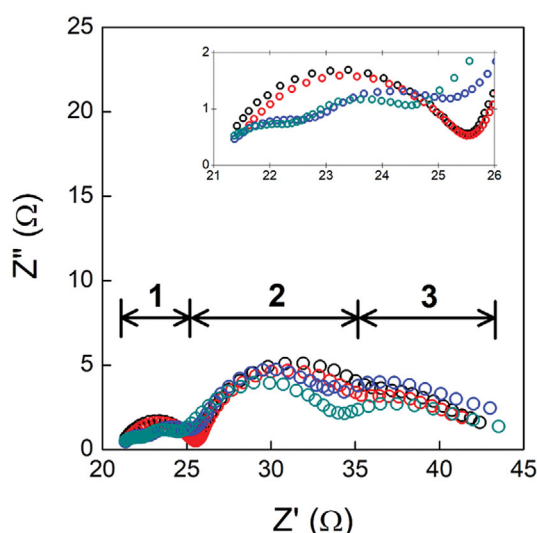
cle diameters in regions 1 and 2, showing that the charge transfer resistance of the photoanode and photocathode strongly depends on whether OMWNTs are employed as key components for both electrodes. The two small semicircles shown in semicircle region 1 are due to diffusional mass transport at high-frequency AC bias in a dense porous polymer network [25,26]. The high-frequency semicircle depends on the charge transfer rate at the counter electrode, FTO/TiO$_2$ interface, and between TiO$_2$ NPs, while the middle-frequency (region 2) and low-frequency (region 3) regimes are affected by the charge transfer process, including electron recombination at the TiO$_2$/N719/electrolyte interface and the Nernst diffusion process involved in the I^-/I_3^- redox reaction [27,28]. The smaller semicircle diameters for DSSC4 at regions 1 and 2 compared to those of the other DSSCs directly indicate faster charge transfer rates at the photoanode and photocathode, enabling DSSC4 to exhibit the best photovoltaic performance. The performance enhancement is larger than that anticipated by considering the results obtained using FTO/TiO$_2$-OMWNTs/N719 or FTO/PEDOT:PSS-OMWNT electrodes. These results are presumably due to back transport and recombination reactions, which commonly occur on the photoanode surface and are effectively suppressed in the full OMWNT-modified PEC system. The EIS data fitting with ZSimp-Win (v. 3.21) is shown in Fig. S2, and all curve-fitting parameters from the results are summarized in Table S1.

CONCLUSIONS

A complete version of an OMWNT-decorated DSSC with a cell structure of FTO/TiO$_2$-OMWNTs/N719//PEDOT:PSS-OMWNTs/FTO displayed the best photovoltaic performance when compared with the other DSSCs. DSSC4 displays a η value that is approximately 6.4% greater than the numerical sum of the efficiencies of DSSCs 2 and 3. The synergistic effect shown using fully OMWNT-modified electrodes appears to be related to the effective suppression of back transport and recombination reactions upon electron harvesting, which was confirmed by comparing the EIS spectra of the corresponding DSSCs. Because the OMWNTs are versatile and applicable to any rigid or flexible/stretchable substrates, their use could be extended to many different research or industrial fields requiring chemical or physical modifications of any type of electrochemical cell, such as secondary batteries, supercapacitors, sensors, and solar cells.

Fig. 5. Nyquist plots of EIS for the various DSSCs in an electrolyte solution composed of 0.6 M 1,2-dimethyl-3-n-propylimidazolium iodide, 0.05 M I$_2$, 0.1 M LiI, and 0.5 M 4-tert-butylpyridine in acetonitrile in the dark. DC Bias=-0.79 V; step potential=5 mV; frequency range=0.1 Hz to 100 kHz. DSSC1 (black), DSSC2 (blue), DSSC3 (red), and DSSC4 (green).

SUPPORTING INFORMATION

Additional information as noted in the text. This information is available via the Internet at http://www.springer.com/chemistry/

journal/11814.

REFERENCES

1. B. O'regan and M. Grätzel, *Nature*, **353**, 737 (1991).
2. I. Mohammadi, F. Zeraatpisheh, E. Ashiri and K. Abdi, *Int. J. Hydrogen Energy*, **45**, 18831 (2020).
3. V. M. Ramakrishnan, S. Pitchaiya, N. Muthukumarasamy, K. Kvamme, G. Rajesh, S. Agilan, A. Pugazhendhi and D. Velauthapillai, *Int. J. Hydrogen Energy*, **45**, 27036 (2020).
4. H. Sayahi, K. Aghapoor, F. Mohsenzadeh, M. M. Morad and H. R. Darabi, *Solar Energy*, **215**, 311 (2021).
5. U. Mehmood, I. A. Hussein, K. Harrabi, M. B. Mekki, S. Ahmed and N. Tabet, *Sol. Energy Mater. Sol. Cells*, **140**, 174 (2015).
6. S. Muduli, W. Lee, V. Dhas, S. Mujawar, M. Dubey, K. Vijayamohanan, S. H. Han and S. Ogale, *ACS Appl. Mater. Interfaces*, **1**, 2030 (2009).
7. Y. H. Rhee, C. J. Lee, M. J. Ko, J. H. Jin and N. K. Min, *J. Phys. Chem. C*, **119**, 9085 (2015).
8. C. Liu, T. Li, Y. Zhang, T. Kong, T. Zhuang, Y. Cui, M. Fang, W. Zhu, Z. Wu and C. Li, *Micropor. Mesopor. Mater.*, **287**, 228 (2019).
9. J. Prakash, S. Sun, H. C. Swart and R. K. Gupta, *Appl. Mater. Today*, **11**, 82 (2018).
10. B. M. Rajbongshi and A. Verma, *Mater. Lett.*, **232**, 220 (2018).
11. B. Roose, S. Pathak and U. Steiner, *Chem. Soc. Rev.*, **44**, 8326 (2015).
12. L. Song, J. Zhai, P. Du, J. Xiong and F. Ko, *Thin Solid Films*, **646**, 44 (2018).
13. B. Ünlü and M. Özacar, *Solar Energy*, **196**, 448 (2020).
14. N. Gao, T. Wan, Z. Xu, L. Ma, S. Ramakrishna and Y. Liu, *Mater. Chem. Phys.*, **255**, 123542 (2020).
15. A. Mathew, G. Mohan Rao and N. Munichandraiah, *Mater. Res. Bull.*, **46**, 2045 (2011).
16. J. M. Pringle, V. Armel and D. R. MacFarlane, *Chem. Commun.*, **46**, 5367 (2010).
17. W. Hong, Y. Xu, G. Lu, C. Li and G. Shi, *Electrochem. Commun.*, **10**, 1555 (2008).
18. K. M. Lee, C. W. Hu, H. W. Chen and K. C. Ho, *Sol. Energy Mater. Sol. Cells*, **92**, 1628 (2008).
19. M. Chang, L. Wu, X. Li and W. Xu, *J. Mater. Sci. Technol.*, **28**, 594 (2012).
20. A. Kongkanand, R. M. Dominguez and P. V. Kamat, *Nano Lett.*, **7**, 676 (2007).
21. C. B. Song, Y. H. Qiang, Y. L. Zhao, X. Q. Gu, D. M. Song and L. Zhu, *Appl. Surf. Sci.*, **305**, 792 (2014).
22. Y. H. Rhee, D. J. Ahn, M. J. Ko, H. Y. Jin, J. H. Jin and N. K. Min, *Electrochim. Acta*, **146**, 68 (2014).
23. Y. Rhee, M. Ko, H. Jin, J. H. Jin and N. K. Min, *Jpn. J. Appl. Phys.*, **53**, 08NJ02-1 (2014).
24. A. Ejigu, K. R. J. Lovelock, P. Licence and D. A. Walsh, *Electrochim. Acta*, **56**, 10313 (2011).
25. J. Bisquert, G. G. Belmonte, F. F. Santiago, N. S. Ferriols, M. Yamashita and E. C. Pereira, *Electrochem. Commun.*, **2**, 601 (2000).
26. F. Fabregat-Santiago, J. Bisquert, G. Garcia-Belmonte, G. Boschloo and A. Hagfeldt, *Sol. Energy Mater. Sol. Cells*, **87**, 117 (2005).
27. N. G. Park, K. M. Kim, M. G. Kang, K. S. Ryu, S. H. Chang and Y. J. Shin, *Adv. Mater.*, **17**, 2349 (2005).
28. Q. Wang, J. E. Moser and M. Gratzel, *J. Phys. Chem. B*, **109**, 14945 (2005).